In-Plane and Out-of-Plane Elastodynamics of Thin Rings and Seals

R. Turnbull[1]
Wolfson School of Mechanical, Electrical and Manufacturing Engineering, Loughborough University, Leicestershire LE11 3TU, UK
e-mail: R.Turnbull@lboro.ac.uk

R. Rahmani
Wolfson School of Mechanical, Electrical and Manufacturing Engineering, Loughborough University, Leicestershire LE11 3TU, UK

H. Rahnejat
Wolfson School of Mechanical, Electrical and Manufacturing Engineering, Loughborough University, Leicestershire LE11 3TU, UK

Thin curved rings used mostly as seals, including in internal combustion engines undergo complex elastodynamic behavior when subjected to a combination of normal radial loading and tangential shear with friction. In turn, their complex modal behavior often results in loss of sealing, increased friction, and power loss. This paper presents a new finite difference approach to determine the response of thin incomplete circular rings. Two interchangeable approaches are presented; one embedding mass and stiffness components in a unified frequency-dependent matrix, and the other making use of equivalent mass and stiffness matrices for the ring structure. The versatility of the developed finite difference formulation can also allow for efficient modification to account for multiple dynamically changing ring support locations around its structure. Very good agreement is observed between the numerical predictions and experimental measurements, particularly with new precision noncontact measurements using laser Doppler vibrometry. The influence of geometric parameters on the frequency response of a high performance motorsport engine's piston compression ring demonstrates the degree of importance of various geometrical parameters on ring dynamic response. [DOI: 10.1115/1.4043526]

Keywords: thin circular ring, seal, elastodynamics, in-plane responses, out-of-plane responses, piston compression ring

1 Introduction

Elastodynamics of thin rings plays an important role in the functional performance of many machines, where they are mostly used for the primary purpose of sealing. For example, thin incomplete circular rings are used as compression rings for sealing the combustion chamber in internal combustion engines. The intention is to guard against the escape of combustion gasses to the bottom-end of the engine. However, effective sealing results in increased friction, while the loss of sealing leads to thermodynamic power loss and lubricant contamination. The compression rings are subjected to a plethora of forces such as contact forces with the cylinder bore surface and with their retaining piston groove lands. There are also applied forces due to radial ring tension, the varying gas force pushing the ring onto the cylinder surface, and friction with the cylinder bore surface. Therefore, in practice the elastodynamic behavior of the compression ring is quite complex and affects its ideal function.

Studying the ring's complex in-plane radial and out-of-plane transversal/axial motions is very important for design analysis purposes. The ring's elastodynamics affects friction, thus the engine's fuel efficiency as well as sealing, hence the engine emissions. A disproportionate 5% of the total engine losses can be attributed to the piston compression ring [1], especially when considering its small size. The thinness of the ring constitutes high modal density, exciting a plethora of responses during the engine cycle, resulting in a number of undesired phenomena such as ring flutter, ring jump, twist, and rotation [2–9], as well as promoting blow-by [10].

A prerequisite for accurate determination of power losses associated with the piston ring system is an understanding of the ring's complex dynamic response. A number of parameters are important, including ring geometry and topography [11,12], ring tension and gas pressure loading [13,14], bore shape and its out-of-roundness [15], and contact kinematics. The dynamic behavior of the ring determines important parameters within a tribological study such as applied loading, contact geometry, and kinematics. In turn, a tribological study of the conjunction provides important input for a ring dynamic analysis [4–6,16] such as the generated contact pressures, load carrying capacity, and friction. Furthermore, the ring's dynamic behavior determines important parameters within a gas flow analysis through the ring pack in an IC engine [2,3,7,8]. This is utilized for the prediction of the phenomena underlying gas blow-by, loss of sealing and power loss, as well as lubricant degradation. Hence, a multiscale, multiphysics study is required, including combined elastodynamics, gas flow, and tribological predictions.

Ejakov et al. [2] demonstrated the effect of ring twist on ring pack performance, noting that the nature of ring twist requires a three-dimensional analysis of the problem. Tian et al. [17] showed that static twist had an impact on ring-groove contact characteristics, dynamic stability, and blow-by. Tian [4] considered a combined ring twist and gas flow model, demonstrating the importance of ring flutter on gas flow and oil transport. However, the transient nature of ring dynamics was not taken into account. Tian [4] noted that the dynamics of the ring significantly affects two important considerations for lubrication on the top two compression rings; oil availability and gas pressure loading. In a two part study Liu et al. [8,9] presented a curved beam finite element method, coupled with a gas dynamic and tribology models to investigate piston ring-pack performance. The importance of the effect of higher combustion pressures, typical of emerging technologies such as cylinder de-activation on friction was demonstrated by Bewsher et al. [18]. However, the effect of gas flow and ring dynamics was not considered in the analysis. Baelden and Tian [19] used the finite element approach for a curved beam to model the compression ring, noting that ring dynamics is an important consideration in any ring-bore conformability analysis such as that undertaken by Mishra et al. [20], who did not consider the dynamics of the ring in their purely localized quasi-static analysis. Consequently, the predicted friction in Ref. [20] showed

[1]Corresponding author.

Contributed by the Design Engineering Division of ASME for publication in the Journal of Computational and Nonlinear Dynamics. Manuscript received January 7, 2019; final manuscript received April 11, 2019; published online May 13, 2019. Assoc. Editor: Tsuyoshi Inoue.

some deviation from measurements of friction by Furuhama and Sasaki [21], which in part may be due to the omission of the transient nature of ring dynamic response. Through successive improvements in their formulation of a ring elastodynamic model, Baker et al. [5–7] were able to show progressive improvements in their numerical predictions against the experimentally obtained measurements by Takiguchi et al. [22]. The fundamental applicability of the well-developed differential equations of motion for thin piston compression rings was demonstrated by Baker et al. [5–7,10]. However, the limitations in the forced response of their dynamic model significantly influenced the consideration of applied forces. For example, in practice, radial forces can adversely influence the transverse ring twist. Conversely, the twist of the ring influences the in situ profile in contact with the liner; thus affecting the radial forces as well as friction, providing a possible insight into the mechanisms of observed asymmetric wear of the ring profile. The development of a ring model that would allow evaluation of localized forces between the ring and the liner at a number of points around the ring without resorting to numerically intensive approaches such as finite element analysis (FEA) is desirable and would be an important extension to the methodology demonstrated in Refs. [5–7] and [10]. This is also the case when considering the applied gas loading and the interaction of the ring with the upper and lower piston retaining lands.

Other essentially thin rings of circular geometry are used in internal combustion engines as oil control rings or in the form of complete circular rings as seals in a host of powertrain or turbomachinery subsystems. Due to the completeness of circumferential geometry the elastodynamic response of these seals deviates from that of the compression rings, but are often subjected to the same plethora of applied forces such as contact loads, lubricant reactions, and friction. Therefore, the study of flexible rings and seals has been of the same importance as those of the compression ring for a long time. Due to long computation times, an ideal closed form analytical solution is preferable, but in practice various approaches have been reported throughout the years.

Earlier analyses include that of Lamb [23] who considered small curved beams, solving an equation for free–free in-plane flexure of a uniform curved bar. Mayer [24] investigated the elasticity and stability of open and closed arcs. Den Hartog [25] extended the work of Lamb [23] to obtain values for the first and second in-plane frequencies of incomplete rings with clamped and hinged boundary conditions. Brown [26] utilized a modification of the Rayleigh's method to determine approximate solutions for out-of-plane vibrations of curved beams and rings. He noted that although an acceptable level of conformance with measurements had been achieved, further investigations were required. Love [27] used the work of Mayer [24] to derive an equation for the natural frequencies of an incomplete circular ring of thin cross section. Archer [28] considered the in-plane forces acting upon an incomplete ring with small cross section in his study of in-plane, in-extensible vibrations for the clamped–clamped boundary conditions. Volterra and Morell [29] determined the lowest in-plane and out-of-plane natural frequencies of elastic arc and elastic hinged arcs. Lang [30,31] further investigated the in-plane ring frequency response, neglecting shear deformation, and rotary inertia. He considered a number of different boundary conditions, extending the investigation of clamped–clamped boundary condition of Archer [28]. Lang [30] noted the difficulty of implementing a ring with multiple supports around its circumference. In particular this would require the modal functions for each ring span between the supports to be defined along with the boundary conditions. Modification of the formulation in this manner is very time consuming and mathematically tedious, limiting the analysis of a combined tribodynamic system. The applicability of Lang's [30] ring model for thin rings and seals was demonstrated by Baker et al. [5–7] to ascertain the influence of ring dynamics on internal combustion engine performance. During the engine cycle, the ring's motion is supported dynamically due to a number of physical constraints dictated by the liner and the piston's upper and lower ring-retaining lands. The developed current methodology is an approach which would allow the implementation of these dynamically changing boundary conditions into a system level analysis. Furthermore, with the advances in modern computational routines for dynamics problems, the mass and stiffness form of the equations is more convenient for solution of natural frequencies and mode shapes than the analytical frequency expressions obtained and solved by Lang [30,31] and Baker et al. [5–7].

Ojalvo [32] utilized a similar method to Morley [33] to analyze the coupled out-of-plane twist and bending vibrations of incomplete rings with clamped–clamped boundary conditions. Rao [34] demonstrated the effect of transverse shear and rotary inertia on the out-of-plane motions of rings. Endo [35] experimentally validated the frequency analysis of complete rings with arbitrary cross section. Hawkings [36] modeled complex complete ring geometries as a series of cross-sectional slices. Yang and Kuo [37] demonstrated the inconsistencies that can occur when a curved beam is represented by several straight beam elements. Furthermore, these inconsistencies have been observed for the piston ring application [38]. Bhimaraddi [39] presented a generalized analysis for laminated rings and curved beams coupling the in-plane and out-of-plane motions. Chidamparam and Leissa [40] conducted a review of the literature into curved beams, rings, and arches deriving equations, including the general case comprising shear correction factors based on the Timoshenko beam theory. Kang et al. [41] utilized the differential quadratic method to investigate the fundamental frequency of in-plane and out-of-plane vibrations, observing good agreement with Ojalvo [32]. Kijun [42] expanded the work of Kang et al. [41] to investigate vibrations of thin-walled curved beams. Challamel et al. [43] investigated the out-of-plane motions of circular arches under different loading conditions. Yang et al. [44] considered curved beams with various curvature forms, such as parabolic, sinusoidal, and elliptical. Shahba et al. [45] also investigated a number of varying curvature rings such as elliptic arches, using an finite element method with new shape functions. The variable curvature approach has been expanded to investigate curved rings made of composite materials [46].

With respect to the specific case of piston compression rings the above historical approaches were initiated for the ring's rigid body dynamic behavior by Tian et al. [17] and the effect of ring dynamics on tribological performance and gas flow dynamics by Dowson et al. [47]. The elastodynamic behavior was first modeled by Ejakov [2] using an FEA model. This was subsequently expanded by Baker et al. [5–7] through an analytical formulation as already noted above, culminating in a complex 3D analysis [7]. Most modern solutions make use of simplified analytical solutions for continuous systems or discretised finite element approaches for thin incomplete circular rings of equivalent rectangular cross section.

A finite difference approach, accounting for material damping, dynamically changing support locations as well as enabling complex application of forces from a combined physics model is essential for the analysis of most modern compression rings. Furthermore, a validated solution against precisely measured ring elastodynamic response is long overdue. Turnbull et al. [48] showed reasonable agreement between numerical predictions of the dynamic response of coupled straight beam elements with experimental frequency sweeps for a ring with a trapezoidal cross section. This work needs to be extended with further comparative studies, particularly for curved incomplete circular rings with rectangular cross section which are often used as piston rings in automotive engines. Thus, the equations of motion are considered to be decoupled, because the plane containing the centreline of the ring axis is the plane of symmetry [40]. These are the main contributions of this paper, providing generic predictions, validated by the state of the art experimental measurements, including the solution demonstrated in mass and stiffness form. The advantage of the developed mass-stiffness formulation here is that it is generic

in nature and can potentially be applied to both coupled and uncoupled ring in-plane and out-of-plane dynamics.

2 Problem Formulation

2.1 Ring In-Plane Dynamics. Figure 1 shows a thin ring, with the definitions of all terms used in the methodology expounded here, as well as the employed co-ordinate system and the in-plane applied forces and moments acting on a ring element.

The following assumptions are made in the derivation of the in-plane motions of a circular ring or a ring segment:

- Rotary inertia and shear deformation are neglected.
- The ring cross section remains constant (unaltered).
- The undeformed ring or ring segment centreline follows either a full circle or a circular arc.
- There are no boundary conditions applied to the ring segment.

Therefore, using Fig. 1, the in-plane equations of motion for a ring segment are obtained as [30]

$$-\frac{EI_1}{R^4}\left(\frac{\partial^3 w}{\partial\theta^3}+\frac{\partial^4 u}{\partial\theta^4}\right)+\frac{EA}{R^2}\left(-u+\frac{\partial w}{\partial\theta}\right)=\rho A\frac{\partial^2 u}{\partial t^2}-f \tag{1}$$

$$\frac{EA}{R^2}\left(-\frac{\partial u}{\partial\theta}+\frac{\partial^2 w}{\partial\theta^2}\right)+\frac{EI_1}{R^4}\left(\frac{\partial^2 w}{\partial\theta^2}+\frac{\partial^3 u}{\partial\theta^3}\right)=\rho A\frac{\partial^2 w}{\partial t^2}-p \tag{2}$$

where ρ and E are the density and Young's modulus of elasticity of the ring material, I_1 is the second area moment of inertia of the ring cross section with respect to the u axis, A is the cross-sectional area, R is the ring radius, θ is the circumferential angular position along the ring, t is time, f is the radially applied in-plane force, p is the tangentially applied in-plane force, u is the radial in-plane deflection, and w is the circumferential in-plane deflection.

As explained in detail by Lang [30], the coupled in-plane Eqs. (1) and (2) can be rewritten in operator notation. Therefore, either of these equations can be expanded, resulting in a differential equation in terms of displacements u or w as follows:

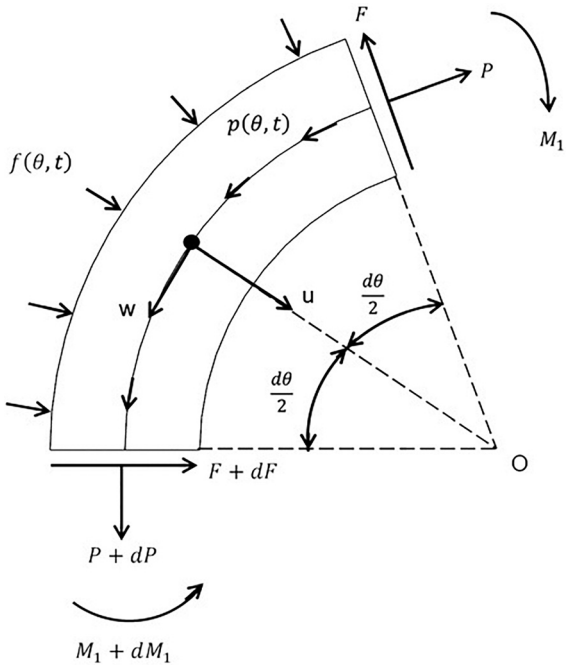

Fig. 1 Definition of a ring in-plane co-ordinate system and geometry

$$\frac{\partial^6\psi}{\partial\theta^6}+2\frac{\partial^4\psi}{\partial\theta^4}+\frac{\partial^2\psi}{\partial\theta^2}+\frac{\rho AR^4}{EI_1}\frac{\partial^2}{\partial t^2}\left(\frac{\partial^2\psi}{\partial\theta^2}-\psi\right),\ \text{where}\ \psi=u\ \text{or}\ w \tag{3}$$

Assuming a harmonic solution with a response frequency, ω, then

$$\psi(\theta,t)=\Psi(\theta)e^{i\omega t} \tag{4}$$

Therefore, in modal coordinates the in-plane equation becomes

$$\frac{\partial^6\Psi}{\partial\theta^6}+2\frac{\partial^4\Psi}{\partial\theta^4}+\frac{\partial^2\Psi}{\partial\theta^2}-\frac{\rho AR^4\omega^2}{EI_1}\left(\frac{\partial^2\Psi}{\partial\theta^2}-\Psi\right)=0 \tag{5}$$

The in-plane dynamic equations can be modified using the Timoshenko beam theory [49,50].

2.2 Ring Out-of-Plane Dynamics. Figure 2 shows a thin ring with the definition of all terms used in the methodology expounded here, as well as the employed co-ordinate system and the out-of-plane forces and moments acting on a ring element/segment.

Based on Fig. 2, and following the assumptions outlined for the in-plane dynamics above, the coupled governing differential equations for the out-of-plane dynamics of a ring including rotary inertia becomes [49]

$$-\frac{EI_2}{R^4}\frac{\partial^4 v}{\partial\theta^4}+\frac{GJ}{R^4}\frac{\partial^2 v}{\partial\theta^2}+\frac{GJ}{R^3}\frac{\partial^2\Omega}{\partial\theta^2}+\frac{EI_2}{R^3}\frac{\partial^2\Omega}{\partial\theta^2}=\rho A\frac{\partial^2 v}{\partial t^2}-q \tag{6}$$

$$\frac{GJ}{R^3}\frac{\partial^2 v}{\partial\theta^2}+\frac{GJ}{R^2}\frac{\partial^2\Omega}{\partial\theta^2}-\frac{EI_2}{R^2}\Omega+\frac{EI_2}{R^3}\frac{\partial^2 v}{\partial\theta^2}=\rho J\frac{\partial^2\Omega}{\partial t^2}-m_0 \tag{7}$$

where ρ and E are the density and Young's modulus of elasticity of the ring material, I_2 is the second area moment of inertia of the cross section with respect to the v axis, A is the cross-sectional area, R is the ring radius, θ is the circumferential angular position along the ring, t is the time, q is the transversally applied out-of-plane force, m_0 is the applied out-of-plane torque, v is the transverse out-of-plane deflection, and Ω is the out-of-plane twist deflection.

Neglecting the effect of rotary inertia, Eqs. (6) and (7) become [49]

$$-\frac{EI_2}{R^4}\frac{\partial^4 v}{\partial\theta^4}+\frac{GJ}{R^4}\frac{\partial^2 v}{\partial\theta^2}+\frac{GJ}{R^3}\frac{\partial^2\Omega}{\partial\theta^2}+\frac{EI_2}{R^3}\frac{\partial^2\Omega}{\partial\theta^2}=\rho A\frac{\partial^2 v}{\partial t^2}-q \tag{8}$$

$$\frac{GJ}{R^3}\frac{\partial^2 v}{\partial\theta^2}+\frac{GJ}{R^2}\frac{\partial^2\Omega}{\partial\theta^2}-\frac{EI_2}{R^2}\Omega+\frac{EI_2}{R^3}\frac{\partial^2 v}{\partial\theta^2}=-m_0 \tag{9}$$

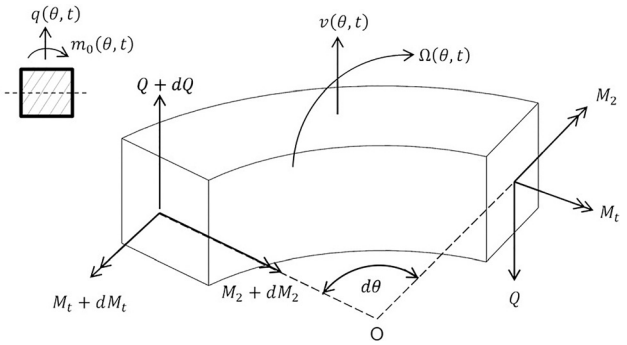

Fig. 2 Definition of a ring out-of-plane co-ordinate system

The coupled out-of-plane differential Eqs. (8) and (9) can be written in operator notation, resulting in differential equations in terms of displacement ν as [49]

$$\frac{\partial^6 v}{\partial\theta^6}+2\frac{\partial^4 v}{\partial\theta^4}+\frac{\partial^2 v}{\partial\theta^2}+\frac{\rho AR^4}{EI_2}\frac{\partial^4 v}{\partial\theta^2\partial t^2}-\frac{\rho AR^4}{GJ}\frac{\partial^2 v}{\partial t^2}=0 \tag{10}$$

The twist Ω is related to the transverse deflection ν as [49]

$$\frac{\partial^2\Omega}{\partial\theta^2}=\frac{1}{EI_2+GJ}\left(\frac{EI_2}{R}\frac{\partial^4 v}{\partial\theta^4}-\frac{GJ}{R}\frac{\partial^2 v}{\partial\theta^2}+\rho AR^3\frac{\partial^2 v}{\partial t^2}-R^3 q\right) \tag{11}$$

Assuming a harmonic solution with the response frequency, ω, then

$$v(\theta,t)=V(\theta)e^{i\omega t} \tag{12}$$

And in modal coordinates, the out-of-plane equation becomes

$$\frac{\partial^6 V}{\partial\theta^6}+2\frac{\partial^4 V}{\partial\theta^4}+\frac{\partial^2 V}{\partial\theta^2}+\frac{\rho AR^4\omega^2}{EI_2}\frac{\partial^2 V}{\partial\theta^2}-\frac{\rho AR^4\omega^2}{GJ}=0 \tag{13}$$

The out-of-plane dynamics equations can be modified using the Timoshenko beam theory [34].

3 Method of Solution

The modal Eqs. (5) and (13) for in-plane and out-of-plane motions, as well as the coupled Eqs. (1) and (2) for in-plane motions and Eqs. (6) and (7) for out-of-plane motions are discretized using a central finite difference method (FDM). A mesh independency study was undertaken to ensure the validity of the results. The mathematical descriptions of the clamped and free boundary conditions at the incomplete ring-ends, as described in Refs. [30–32] and [34], are implemented in the modal equations at the boundary. This allows mesh points which are outside the boundary to be mathematically represented by the points within the boundary of the incomplete ring.

Discretizing Eqs. (5) and (13), using finite difference method, yields a frequency-dependent matrix containing both mass and stiffness contributions for the in-plane and out-of-plane vibrations, respectively. Formulation of the frequency-dependent coefficient matrix for modal equations is provided in the Appendices A and B for both the in-plane and out-of-plane dynamics, respectively. The solution for the natural modal frequencies, ω_n of the system are found, when the determinant of the eigenmatrix vanishes.

For in-plane vibrations

$$\det(\mathbf{A})=0 \tag{14}$$

and for out-of-plane vibrations

$$\det(\mathbf{B})=0 \tag{15}$$

The modal displacements associated with each individual value of ω_n are found by substituting each calculated value of ω_n back into the relevant matrix: **A** or **B**.

The equations of motion (1) and (2) for the in-plane motions and (6) and (7) for the out-of-plane motions, discretized using FDM, can be rearranged and combined in order to obtain the equivalent mass (**M**) and the stiffness (**K**) matrices. Therefore, it is possible to combine the equations for in-plane and out-of-plane motions and represent them in a conventional mass matrix form, where

$$\boldsymbol{M}_g=\begin{bmatrix}\boldsymbol{M}_{ip} & 0\\ 0 & \boldsymbol{M}_{op}\end{bmatrix} \tag{16}$$

and

$$\boldsymbol{K}_g=\begin{bmatrix}\boldsymbol{K}_{ip} & 0\\ 0 & \boldsymbol{K}_{op}\end{bmatrix} \tag{17}$$

The mass and stiffness formulation can then be easily solved for the natural frequencies of the system, where **M** and **K** represent the corresponding characteristic mass and stiffness matrices of the structure, thus

$$|\mathbf{K}-\mathbf{M}\lambda_n|=0 \tag{18}$$

where

$$\lambda_n=\omega^2 \tag{19}$$

The resultant mode shapes of the system are found through solution of

$$(\mathbf{K}-\mathbf{M}\lambda_n)\{\mathbf{x}_n\}=\mathbf{0} \tag{20}$$

where the term ω_n is the nth natural frequency of vibrations of the system, and $\mathbf{x}_n$ is its associated modal displacement vector. Formulations of the mass and stiffness matrices are given in Appendices C and D for the in-plane and the out-of-plane dynamics, respectively.

4 Experimental Investigation

Experimentally measured responses of a piston compression ring of a modern high performance race engine are carried out. A ring of rectangular cross section is chosen for the current investigation as it allows the in-plane and out-of-plane deformations to be decoupled as there is no common degree-of-freedom between the in-plane and out-of-plane motions [7,30,32,49]. The ring specifications are listed in Table 1 and Fig. 3.

The experimental rig comprises a clamped-free incomplete circular piston compression ring of rectangular cross section, rigidly clamped at one extremity of its end-gap to a vibration exciter, and with the other opposing end-gap remaining unconstrained to vibrate freely. Previous experiments [30,31] have relied on the use of miniature accelerometers positioned on the ring. These physically add mass to the thin low mass vibrating structure, thus affecting its modal responses. Laser Doppler vibrometers (LDV) are ideally suited for noncontact measurement of such vibrating

Table 1 Experimental ring specifications

Ring material		
Modulus of elasticity	210	GPa
Density	7850	kg/m^3
Poisson's ratio	0.3	–
Ring dimensions		
Inner radius, R_0	43	mm
Axial height, h_0	1.15	mm
Radial width, w_0	3.5	mm
Ring free end gap, e_0	6	mm

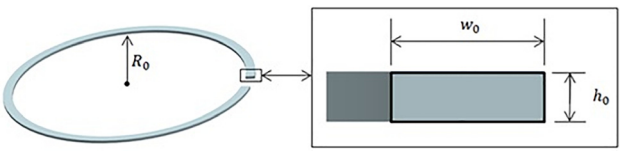

Fig. 3 Schematic of ring cross section

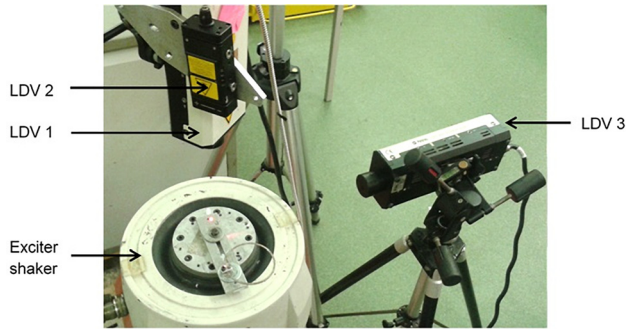

Fig. 4 The experimental setup

Table 2 Instrumentation

Apparatus	Measurement sensitivity	Amplifier setup sensitivity
Excitation laser (LDV 1) (OFV-400)	14 mm/s/V	14 mm/s/V
Piston ring response laser (LDV 2) (RLV-5500)	200 mm/s/V	200 mm/s/V
Excitation laser (LDV 3) (OFV-400)	14 mm/s/V	14 mm/s/V

Table 3 Complete ring specifications

Ring material		
Modulus of elasticity	210	GPa
Density	7850	kg/m^3
Poisson's ratio	0.3	–
Ring dimensions		
Inner radius	43	mm
Axial height	1.15	mm
Radial width	3.5	mm

structures. They are used in the current experimental setup (Fig. 4). The LDVs monitor a Doppler shift in the frequency of light scattered by the moving object [51].

The LDV 1 (model: OFV-400) and LDV 3 (model: OFV-400) are positioned in order to measure the applied excitation by the shaker at the rigidly clamped ring's end-gap interface. The LDV 2 (model: RLV-5500) is positioned to measure the ring response at its free end-gap. A frequency sweep excitation in the range 10–500 Hz is carried out over a period of 10 s. The Nyquist criterion dictates a sampling rate at least twice that of the highest expected response frequency. Therefore, a conservative sampling rate of 8000 Hz is used. Table 2 details the instrumentation utilized in the experiment. Further details on the experimental approach can be found in Ref. [48].

5 Results and Discussion

5.1 Validation of Methodology. To validate the expounded numerical method, the equations of motion (1) and (2) for in-plane motions and (6) and (7) for out of plane motions are initially solved for the simple case of a closed complete circular ring. This problem has a closed form analytical solution for its frequency response. Frequency analysis is completed on the mass and stiffness equations for a complete ring detailed in Table 3, of similar structure to the incomplete ring (detailed in Table 1) without the ring free end gap and compared with the analytical frequency expressions, reported in Ref. [49].

For in-plane vibrations, the natural frequencies are given by

$$\omega_n^2 = \frac{EI_1}{\rho AR^4}\frac{n^6 - 2n^4 + n^2}{n^2 + 1} \tag{21}$$

In addition, for out-of-plane vibrations the natural frequencies are

$$\omega_n^2 = \frac{EI_2}{\rho AR^4}\frac{n^6 - 2n^4 + n^2}{n^2 + EI_2/GJ} \tag{22}$$

where

$$\omega_n = 2\pi f_v \tag{23}$$

As shown in Table 4, the absolute percentage error between the current numerical solution and the closed form analytical solution in Ref. [49] never exceed 0.32% for the first 11 response modes. This approach imparts a good degree of confidence with regard to the expounded numerical methodology.

The predicted mode shapes associated with the first three in-plane and out-of-plane natural frequencies in Table 4 for a complete ring (with specifications given in Table 3) are presented in Fig. 5.

The next step in the validation process involves comparison of in-plane modal predictions with experimental measurements reported by Lang [30,31] for in-plane flexural vibrations of a flexible ring, point-clamped rigidly to a vibration exciter. The shaker excitation was measured by attaching a piezoelectric accelerometer to the armature of the shaker and the response of the ring was recorded by attaching a piezoelectric accelerometer to the circumference of the ring in order to measure its radial acceleration [30,31]. Here, the clamped boundary condition is applied to both the incomplete ring's end-gap extremities. Table 5 lists the specifications for the ring used in Refs. [30] and [31].

Table 6 provides comparisons between the experimental results of Lang [30,31] and the predictions of the current model. The maximum percentage difference is recorded at 1%, demonstrating excellent conformance of the predictions with the measurements

Table 4 Comparison between the current predictions and the closed form solution

Mode	Analytical [44] (Hz)	Current analysis (Hz)	Plane of vibration	Error (%)
1	430.0	428.6	Out-of-plane	−0.32
2	1166.1	1162.9	Out-of-plane	−0.28
3	1207.0	1207.5	In-plane	0.04
4	2199.6	2193.7	Out-of-plane	−0.27
5	3413.9	3407.0	In-plane	−0.20
6	3529.3	3519.9	Out-of-plane	−0.26
7	5154.8	5141.1	Out-of-plane	−0.27
8	6545.8	6528.9	In-plane	−0.26
9	7076.0	7057.0	Out-of-plane	−0.27
10	9292.8	9267.5	Out-of-plane	−0.27
11	10586.0	10556.0	In-plane	−0.28

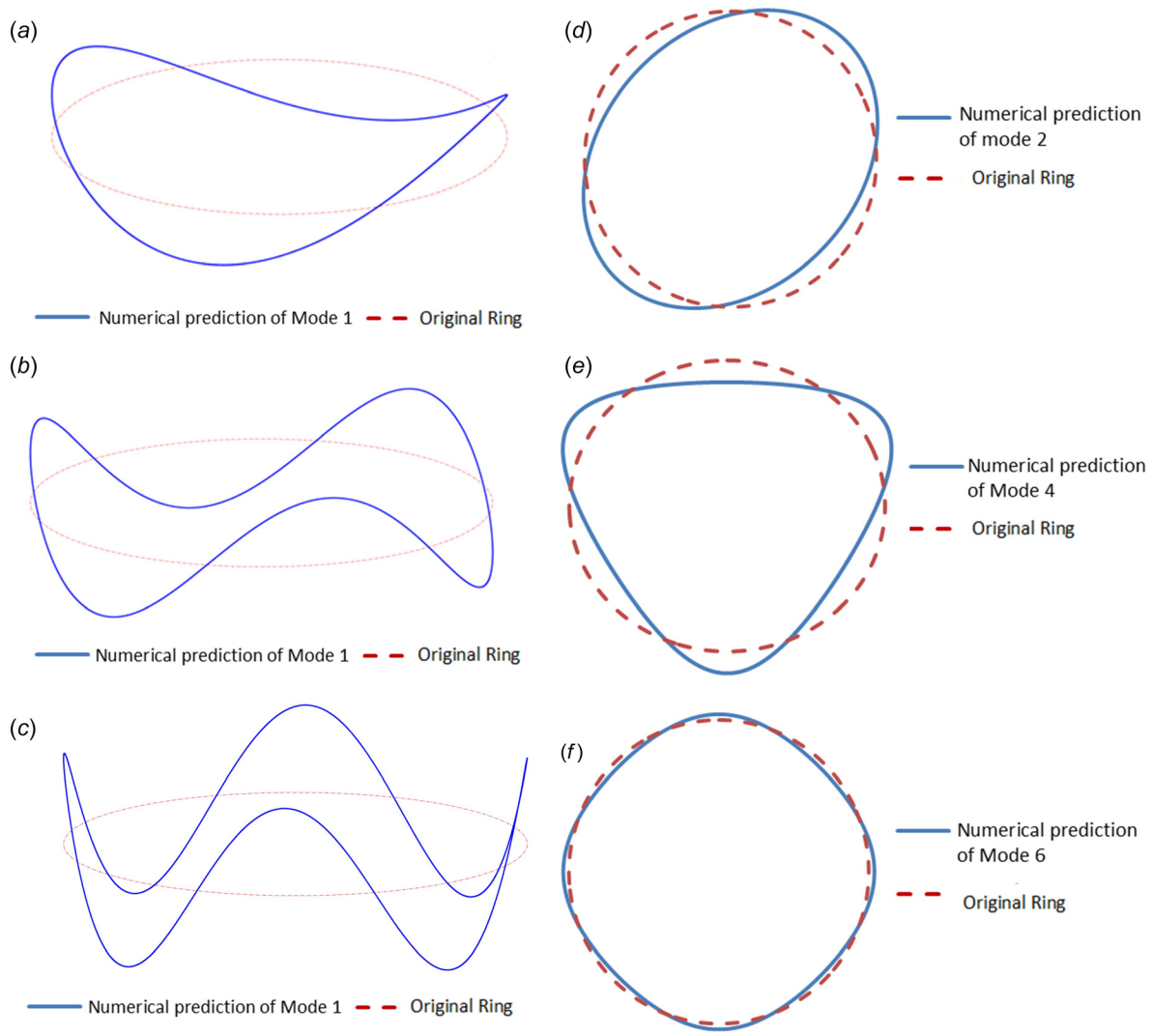

Fig. 5 Predicted in-plane mode shapes: (*a*) 1207.5 Hz, (*b*) 3407.0 Hz, and (*c*) 6528.9 Hz and predicted out-of-plane mode shapes (*d*) 428.6 Hz, (*e*) 1162.9 Hz, and (*f*) 2193.7 Hz

Table 5 Complete ring specification used by Lang [30,31]

Ring material		
Modulus of elasticity	210	GPa
Density	7850	kg/m^3
Poisson's ratio	0.3	–
Ring dimensions		
Inner radius	254	mm
Height	25.4	mm
Width	6.35	mm

in Refs. [30] and [31]. This imparts further confidence on the developed methodology for the solution of the modal equations, including for the clamped boundary conditions applied to both the ring's end-gap extremities.

In addition, the corresponding mode shapes, associated with the modal frequencies outlined in Table 6, are provided in Fig. 6. Good agreement is achieved between the predicted numerical mode shapes and the experimental measurements obtained by Lang [30,31].

5.2 Combined Experimental and Numerical Investigation of High Performance Piston Compression Ring Elastodynamics. The experimental measurements for an ultra-thin modern compression ring of a high performance motorsport race engine (Table 7) are presented, alongside the predicted numerical frequencies for the first nine natural modes. The clamped boundary

Table 6 Comparison of current predictions with the experimental measurements of Lang [30,31]

Mode number	Experimental measurements [28,29] (Hz)	Current predictions (Hz)	Percentage error (%)
1	40	39.6	1
2	140	141.3	−0.93
3	296	296.7	−0.24

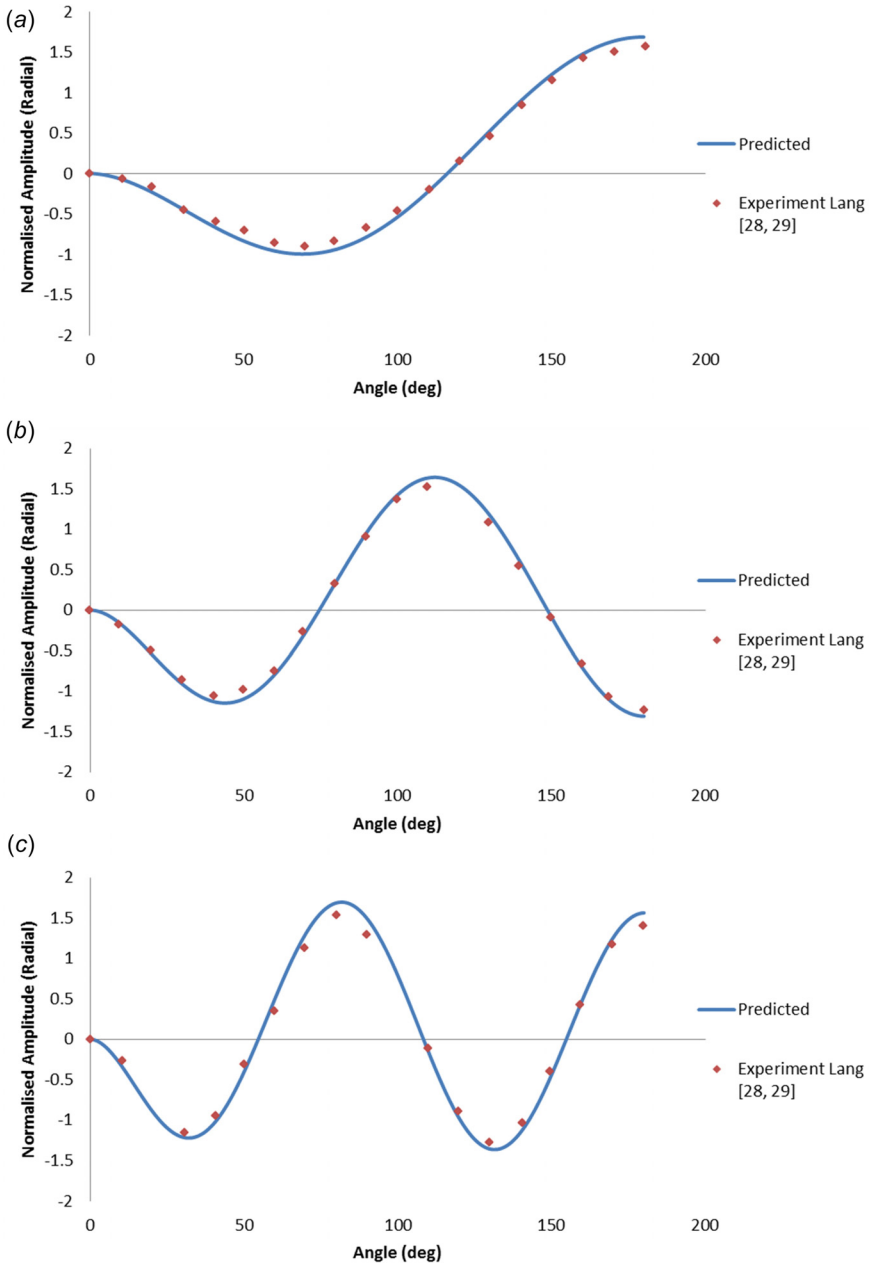

Fig. 6 Comparison of the predicted and measured mode shapes for: (*a*) 40 Hz, (*b*) 140 Hz, and (*c*) 296 Hz

Table 7 Comparison of the in-plane and out-of-plane modes between predictions and measurements for the thin compression ring

Experiment (Hz)	Numerical (Hz)	Plane of motion	Error (%)
129.8	125	Out-of-plane	−3.70
250.9	262	In-plane	4.42
294.4	289	Out-of-plane	−1.83
562.7	588	Out-of-plane	4.50
761.3	738	In-plane	−3.06
914.7	944	Out-of-plane	3.20
1361.1	1402	Out-of-plane	3.00
1642.5	1560	In-plane	−5.02
2028.2	1915	Out-of-plane	−5.58

condition is applied to one of the incomplete ring's end-gap extremities with the free boundary condition applied to the other free end. Table 1 and Fig. 4 (Sec. 4) represent the studied case.

Important geometrical design attributes for the piston compression ring are its radius (R_0), radial width (w_0), axial height (h_0), and ring free end gap (e_0). These geometric properties can have a significant impact on the piston compression ring's frequency response. Figure 7 demonstrates the importantance of these geometric properties on the piston compresion ring, where the original parameters are R_0, w_0, h_0, and e_0 given in Table 1. The nondimensional parameter (d_*) represents the ratio of altered ring parameter to its original value. The nondimensional frequency ratio (f_*) is

$$f_* = \frac{f}{f_0} \tag{24}$$

where f_0 is the original frequency of the structure.

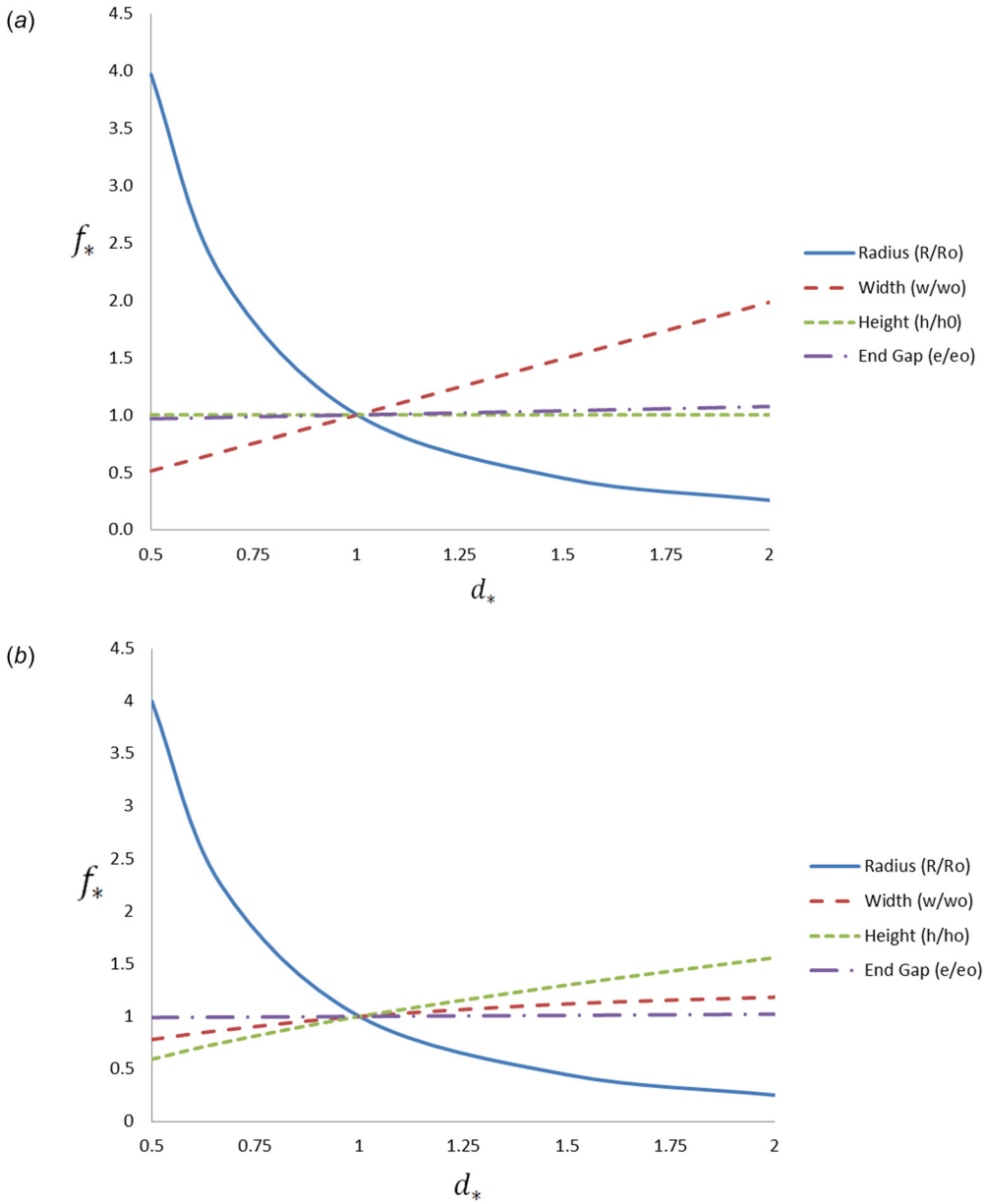

Fig. 7 Nondimensional design analysis: the effect of geometric properties on: (*a*) in-plane and (*b*) out-of-plane frequency responses

Figure 7 demonstrates how the structural vibrations of thin rings and seals can be affected by the geometric properties. Alterations to fundamental frequency response of the structure can be important in certain applications whereby the ring's resonance frequency coincides with other operational frequencies, compromising some ideal function. As it can be seen from Fig. 7, ring radius is the most significant geometric property in the frequency response of the piston compression ring, compared with other geometrical parameters in terms of impacting the frequency response. Any change in the ring width ratio also causes significant changes in the ring in-plane frequency response. However, this parameter has less of an effect in the case of out-of-plane frequency response. In the case of out-of-plane dynamics, the height ratio appears to be more significant than the width ratio. The ring end-gap has minimal effect on both the in-plane and out-of-plane frequency responses. Furthermore, with regard to the cross-sectional parameters, the in-plane frequency response is affected by the ring width, while the ring height shows no significant effect. However, the out-of-plane frequency response is fundamentally governed by both the ring thickness and the ring height. Therefore, it is important to consider both the in-plane and out-of-plane problems together for a number of engineering applications such as the piston compression ring. It is also important to note that the theory demonstrated does not include rotary inertia which can be influential in the solution of thick ring geometries.

6 Conclusions

Accurate determination of complex elastodynamics of rings and seals is a prerequisite for the prediction of sealing performance, comprising leakage, pressure loss, and frictional assessment. The power losses associated with such seals is best demonstrated by the piston compression ring of internal combustion engines. The methodology expounded in this paper has demonstrated applicability for prediction of complex elastodynamic behavior which has been subjected to vigorous validation against closed form solutions of simpler conditions, as well as some measurements reported in the literature. The study is extended to the case

of a thin light compression ring of a high performance race engine using noncontact laser vibrometry and the expounded numerical method. Very good agreement is obtained for the predictions in all cases. The formulation provides a numerically efficient method to include the effect of supports at dynamically changing locations around the ring structure as well as allowing material damping to be included within the analysis. The mass and stiffness formulation is convenient for implementation within a multiphysics environment without investing in numerically intensive approaches such as FEA. The model developed here allows realistic loads to be considered that should provide insight into the fundamental mechanisms of ring flutter, ring jump, twist, and rotation. The influence of geometric properties on the in-plane and out-of-plane frequency response of an ultra-thin modern compression ring of a high performance motorsport race engine is demonstrated. Furthermore, the importance of considering in-plane and out-of-plane vibrations together is highlighted in order to avoid any undesired functional performance. The influence of ring dynamics on engine parasitic losses and emissions is a well-known phenomenon and the current analysis, when combined with ring tribology and gas blow-by analysis, would provide a cost-effective tool for parametric and optimization study of engine component design to achieve maximum sealing ability, while mitigating frictional parasitic losses. From a dynamics perspective the design parameters can be the ring and piston ring-retaining groove geometrical and material properties.

Acknowledgment

The authors would like to acknowledge the financial support of the reported research by the Engineering and Physical Sciences (EPSRC) under the Centre for Doctoral Training in Embedded Intelligence (CDT-EI).

Funding Data

- Engineering and Physical Sciences Research Council (EPSRC) (EP/L014998/1; Funder ID: 10.13039/501100000266).

Nomenclature

A = cross-sectional area, m^2
$\mathbf{A}, \mathbf{B}$ = matrices of coefficients
d_* = geometric ratio
E = Young's modulus of elasticity, $N{\cdot}m^{-2}$
f = radially applied force per unit length, $N{\cdot}m^{-1}$
F = shear force, N
f_v = frequency of vibration, s^{-1}
f_* = frequency ratio
G = shear modulus, $N{\cdot}m^{-2}$
I_1 = second area moment of inertia about the u-axis, m^4
I_2 = second area moment of inertia about the v-axis, m^4
$IP_a - IP_g$ = elements of coefficient matrix for in-plane ring dynamics
J_p = polar area moment of inertia, m^4
$\mathbf{K}$ = stiffness matrix, $N{\cdot}m^{-1}$
$\mathbf{M}$ = mass matrix, kg
m_0 = applied torque per unit length, N
M_t = torsional moment about the tangential axis, N·m
M_1 = in-plane bending moment, N·m
M_2 = bending moment about the radial axis, N·m
$OP_a - OP_g$ = elements of coefficient matrix for out-of-plane ring dynamics
p = tangential applied force per unit length, $N{\cdot}m^{-1}$
P = tensile force, N
q = Transversally applied force per unit length, $N{\cdot}m^{-1}$
Q = transverse shear force, N
R = ring radius, m
t = time, s
u = radial in-plane deflection, m
v = transverse out-of-plane deflection, m
v_p = Poisson's ratio
w = circumferential in-plane deflection, m

Greek Symbols

Δx = discretized interval in the circumferential direction, rad
θ = circumferential angular position along the ring periphery, rad
ξ, ξ_1, ξ_2 = system frequency parameters
ρ = material density, kgm^{-3}
Ψ, ψ = Intermediate parameters
ω = angular radiancy, rad s^{-1}
Ω = out-of-plane twist, rad

Subscripts

g = combined
ip = in-plane
op = out-of-plane

Abbreviations

FDM = finite difference method
FEA = finite element analysis

Appendix A: In-Plane Modal Equation for Each Single Mesh Point

Discretization of Eq. (5) results in a frequency-dependent matrix of coefficients, embodying both the mass and stiffness terms. Hence, the in-plane behavior for point i becomes

$$\begin{bmatrix} \mathrm{IP}_a & \mathrm{IP}_b & \mathrm{IP}_c & \mathrm{IP}_d & \mathrm{IP}_e & \mathrm{IP}_f & \mathrm{IP}_g \end{bmatrix} \begin{bmatrix} \Psi_{i-3} \\ \Psi_{i-2} \\ \Psi_{i-1} \\ \Psi_i \\ \Psi_{i+1} \\ \Psi_{i+2} \\ \Psi_{i+3} \end{bmatrix} = 0 \quad \text{(A1)}$$

where

$$\mathrm{IP}_a = \mathrm{IP}_g = 1 \quad \text{(A2)}$$

$$\mathrm{IP}_b = \mathrm{IP}_f = -6 + 2\Delta x^2 \quad \text{(A3)}$$

$$\mathrm{IP}_c = \mathrm{IP}_e = 15 - 8\Delta x^2 + (1 - \xi)\Delta x^4 \quad \text{(A4)}$$

$$\mathrm{IP}_d = -20 + 12\Delta x^2 - 2(1 - \xi)\Delta x^4 + \xi \Delta x^6 \quad \text{(A5)}$$

and

$$\xi = \frac{\rho A R^4 \omega^2}{E I_1} \quad \text{(A6)}$$

Hence, matrix $\mathbf{A}$

$$\boldsymbol{A} = \begin{bmatrix} \mathrm{IP}_a & \mathrm{IP}_b & \mathrm{IP}_c & \mathrm{IP}_d & \mathrm{IP}_e & \mathrm{IP}_f & \mathrm{IP}_g \end{bmatrix} \quad \text{(A7)}$$

Appendix B: Out-of-Plane Modal Equation for Each Single Mesh Point

Discretisation of Eq. (13) yields a frequency-dependent matrix, embedding both the mass and stiffness terms. Hence, the out-of-plane behavior for a point i becomes

$$\begin{bmatrix} \mathrm{OP}_a & \mathrm{OP}_b & \mathrm{OP}_c & \mathrm{OP}_d & \mathrm{OP}_e & \mathrm{OP}_f & \mathrm{OP}_g \end{bmatrix} \begin{bmatrix} \mathrm{V}_{i-3} \\ \mathrm{V}_{i-2} \\ \mathrm{V}_{i-1} \\ \mathrm{V}_i \\ \mathrm{V}_{i+1} \\ \mathrm{V}_{i+2} \\ \mathrm{V}_{i+3} \end{bmatrix} = 0 \tag{B1}$$

where

$$\mathrm{OP}_a = \mathrm{OP}_g = 1 \tag{B2}$$

$$\mathrm{OP}_b = \mathrm{OP}_f = -6 + 2\Delta x^2 \tag{B3}$$

$$\mathrm{OP}_c = \mathrm{OP}_e = 15 - 8\Delta x^2 + (1 - \xi_1)\Delta x^4 \tag{B4}$$

$$\mathrm{OP}_d = -20 + 12\Delta x^2 - 2(1 - \xi_1)\Delta x^4 + \xi_2 \Delta x^6 \tag{B5}$$

and

$$\xi_1 = \frac{\rho A R^4 \omega^2}{E I_2} \tag{B6}$$

$$\xi_2 = \frac{\rho A R^4 \omega^2}{GJ} \tag{B7}$$

Hence, matrix $\mathbf{B}$

$$\mathbf{B} = \begin{bmatrix} \mathrm{OP}_a & \mathrm{OP}_b & \mathrm{OP}_c & \mathrm{OP}_d & \mathrm{OP}_e & \mathrm{OP}_f & \mathrm{OP}_g \end{bmatrix} \tag{B8}$$

Appendix C: In-Plane Dynamics Formulation in Mass and Stiffness Matrix Form

Discretization of Eqs. (1) and (2) provides the mass and stiffness terms for the in-plane elastodynamic behavior.

The in-plane inertial forces for point i, take the form

$$\begin{bmatrix} M_u & 0 \\ 0 & M_w \end{bmatrix} \begin{bmatrix} \ddot{u}_i \\ \ddot{w}_i \end{bmatrix} \tag{C1}$$

Hence, the mass matrix $\boldsymbol{M}_{\mathrm{ip}}$

$$\boldsymbol{M}_{ip} = \begin{bmatrix} M_u & 0 \\ 0 & M_w \end{bmatrix} \tag{C2}$$

where, the elements of the mass matrix are

$$M_u = \rho A R \tag{C3}$$

$$M_w = \rho A R \tag{C4}$$

Thus, the in-plane elastic force for point i, takes the form

$$\begin{bmatrix} K_{uu-2} & K_{uw-2} & K_{uu-1} & K_{uw-1} & K_{uu} & K_{uw} & K_{uu+1} & K_{uw+1} & K_{uu+2} & K_{uw+2} \\ K_{wu-2} & K_{ww-2} & K_{wu-1} & K_{ww-1} & K_{wu} & K_{ww} & K_{wu+1} & K_{ww+1} & K_{wu+2} & K_{ww+2} \end{bmatrix} \begin{bmatrix} u_{i-2} \\ w_{i-2} \\ u_{i-1} \\ w_{i-1} \\ u_i \\ w_i \\ u_{i+1} \\ w_{i+1} \\ u_{i+2} \\ w_{i+2} \end{bmatrix} \tag{C5}$$

Hence, the stiffness matrix $\boldsymbol{K}_{\mathrm{ip}}$ becomes

$$\boldsymbol{K}_{\mathrm{ip}} = \begin{bmatrix} K_{uu-2} & K_{uw-2} & K_{uu-1} & K_{uw-1} & K_{uu} & K_{uw} & K_{uu+1} & K_{uw+1} & K_{uu+2} & K_{uw+2} \\ K_{wu-2} & K_{ww-2} & K_{wu-1} & K_{ww-1} & K_{wu} & K_{ww} & K_{wu+1} & K_{ww+1} & K_{wu+2} & K_{ww+2} \end{bmatrix} \tag{C6}$$

where the stiffness constants are

$$K_{uu-2} = -\frac{1}{\Delta x^4}\frac{E I_1}{R^3} \tag{C7}$$

$$K_{uw-2} = \frac{1}{2\Delta x^3}\frac{E I_1}{R^3} - \frac{1}{2\Delta x}\frac{EA}{R} \tag{C8}$$

$$K_{uu-1} = \frac{4}{\Delta x^4}\frac{E I_1}{R^3} \tag{C9}$$

$$K_{uw-1} = -\frac{1}{\Delta x^3}\frac{E I_1}{R^3} \tag{C10}$$

$$K_{uu} = -\frac{6}{\Delta x^4}\frac{E I_1}{R^3} - \frac{EA}{R} \tag{C11}$$

$$K_{uw} = 0 \tag{C12}$$

$$K_{uu+1} = \frac{4}{\Delta x^4}\frac{\mathrm{EI}_1}{R^3} \tag{C13}$$

$$K_{uw+1} = \frac{1}{\Delta x^3}\frac{E I_1}{R^3} + \frac{1}{2\Delta x}\frac{EA}{R} \tag{C14}$$

$$K_{uu+2} = -\frac{1}{\Delta x^4}\frac{E I_1}{R^3} \tag{C15}$$

$$K_{uw+2} = -\frac{1}{2\Delta x^3}\frac{EI_1}{R^3} \tag{C16}$$

$$K_{wu-2} = -\frac{1}{2\Delta x^3}\frac{EI_1}{R^3} \tag{C17}$$

$$K_{ww-2} = 0 \tag{C18}$$

$$K_{wu-1} = \frac{1}{\Delta x^3}\frac{EI_1}{R^3} + \frac{1}{2\Delta x}\frac{EA}{R} \tag{C19}$$

$$K_{ww-1} = \frac{1}{\Delta x^2}\frac{EI_1}{R^3} + \frac{1}{\Delta x^2}\frac{EA}{R} \tag{C20}$$

$$K_{wu} = 0 \tag{C21}$$

$$K_{ww} = -\frac{2}{\Delta x^2}\frac{EI_1}{R^3} - \frac{2}{\Delta x^2}\frac{EA}{R} \tag{C22}$$

$$K_{wu+1} = -\frac{1}{\Delta x^3}\frac{EI_1}{R^3} - \frac{1}{2\Delta x}\frac{EA}{R} \tag{C23}$$

$$K_{ww+1} = \frac{1}{\Delta x^2}\frac{EI_1}{R^3} + \frac{1}{\Delta x^2}\frac{EA}{R} \tag{C24}$$

$$K_{wu+2} = \frac{1}{2\Delta x^3}\frac{EI_1}{R^3} \tag{C25}$$

$$K_{ww+2} = 0 \tag{C26}$$

Appendix D: Out-of-Plane Dynamics Formulation in Mass and Stiffness Matrix Form

Discretization of Eqs. (6) and (7) provides the mass and stiffness terms for out-of-plane dynamic behavior.

The out-of-plane inertial forces for point i, takes the form

$$\begin{bmatrix} M_v & 0 \\ 0 & M_\Omega \end{bmatrix} \begin{bmatrix} \ddot{v}_i \\ \ddot{\Omega}_i \end{bmatrix} \tag{D1}$$

Hence, the mass matrix $\boldsymbol{M}_{\text{op}}$

$$\boldsymbol{M}_{op} = \begin{bmatrix} M_v & 0 \\ 0 & M_\Omega \end{bmatrix} \tag{D2}$$

where the elements are given by

$$M_v = \rho AR \tag{D3}$$

$$M_\Omega = \rho JR \tag{D4}$$

The out-of-plane elastic force for point i, takes the form

$$\begin{bmatrix} K_{vv-2} & K_{v\Omega-2} & K_{vv-1} & K_{v\Omega-1} & K_{vv} & K_{v\Omega} & K_{vv+1} & K_{v\Omega+1} & K_{vv+2} & K_{v\Omega+2} \\ K_{\Omega v-2} & K_{\Omega\Omega-2} & K_{\Omega v-1} & K_{\Omega\Omega-1} & K_{\Omega v} & K_{\Omega\Omega} & K_{\Omega v+1} & K_{\Omega\Omega+1} & K_{\Omega v+2} & K_{\Omega\Omega+2} \end{bmatrix} \begin{bmatrix} v_{i-2} \\ \Omega_{i-2} \\ v_{i-1} \\ \Omega_{i-1} \\ v_i \\ \Omega_i \\ v_{i+1} \\ \Omega_{i+1} \\ v_{i+2} \\ \Omega_{i+2} \end{bmatrix} \tag{D5}$$

Hence, the stiffness matrix $\boldsymbol{K}_{\text{op}}$

$$\boldsymbol{K}_{op} = \begin{bmatrix} K_{vv-2} & K_{v\Omega-2} & K_{vv-1} & K_{v\Omega-1} & K_{vv} & K_{v\Omega} & K_{vv+1} & K_{v\Omega+1} & K_{vv+2} & K_{v\Omega+2} \\ K_{\Omega v-2} & K_{\Omega\Omega-2} & K_{\Omega v-1} & K_{\Omega\Omega-1} & K_{\Omega v} & K_{\Omega\Omega} & K_{\Omega v+1} & K_{\Omega\Omega+1} & K_{\Omega v+2} & K_{\Omega\Omega+2} \end{bmatrix} \tag{D6}$$

where, the stiffness constants are

$$K_{vv-2} = -\frac{1}{\Delta x^4}\frac{EI_2}{R^3} \tag{D7}$$

$$K_{v\Omega-2} = 0 \tag{D8}$$

$$K_{vv-1} = \frac{4}{\Delta x^4}\frac{EI_2}{R^3} + \frac{1}{\Delta x^2}\frac{GJ}{R^3} \tag{D9}$$

$$K_{v\Omega-1} = \frac{1}{\Delta x^2}\frac{EI_2}{R^2} + \frac{1}{\Delta x^2}\frac{GJ}{R^2} \tag{D10}$$

$$K_{vv} = -\frac{6}{\Delta x^4}\frac{EI_2}{R^3} - \frac{2}{\Delta x^2}\frac{GJ}{R^3} \tag{D11}$$

$$K_{v\Omega} = -\frac{1}{\Delta x^2}\frac{EI_2}{R^2} - \frac{2}{\Delta x^2}\frac{GJ}{R^2} \tag{D12}$$

$$K_{vv+1} = \frac{4}{\Delta x^4}\frac{EI_2}{R^3} + \frac{1}{\Delta x^2}\frac{GJ}{R^3} \tag{D13}$$

$$K_{v\Omega+1} = \frac{1}{\Delta x^2}\frac{EI_2}{R^2} + \frac{1}{\Delta x^2}\frac{GJ}{R^2} \tag{D14}$$

$$K_{vv+2} = -\frac{1}{\Delta x^4}\frac{EI_2}{R^3} \tag{D15}$$

$$K_{v\Omega+2} = 0 \tag{D16}$$

$$K_{\Omega v-2} = 0 \tag{D17}$$

$$K_{\Omega\Omega-2} = 0 \tag{D18}$$

$$K_{\Omega v-1} = \frac{1}{\Delta x^2}\frac{EI_2}{R^2} + \frac{1}{\Delta x^2}\frac{GJ}{R^2} \tag{D19}$$

$$K_{\Omega\Omega-1} = \frac{1}{\Delta x^2}\frac{GJ}{R} \tag{D20}$$

$$K_{\Omega v} = -\frac{2}{\Delta x^2}\frac{EI_2}{R^2} - \frac{2}{\Delta x^2}\frac{GJ}{R^2} \tag{D21}$$

$$K_{\Omega\Omega} = -\frac{EI_2}{R} - \frac{2}{\Delta x^2}\frac{GJ}{R} \tag{D22}$$

$$K_{\Omega v+1} = \frac{1}{\Delta x^2}\frac{EI_2}{R^2} + \frac{1}{\Delta x^2}\frac{GJ}{R^2} \tag{D23}$$

$$K_{\Omega\Omega+1} = \frac{1}{\Delta x^2}\frac{GJ}{R} \tag{D24}$$

$$K_{\Omega v+2} = 0 \tag{D25}$$

$$K_{\Omega\Omega+2} = 0 \tag{D26}$$

References

[1] Andersson, B. S., 1991, "Company Perspectives in Vehicle Tribology-Volvo," Tribol. Ser., **18**, pp. 503–506.

[2] Ejakov, M. A., Schock, H. J., and Brombolich, L. J., 1998, "Modeling of Ring Twist for an IC Engine," SAE Paper No. 982693.

[3] Tian, K.-T., 2002, "Dynamic Behaviours of Piston Rings and Their Practical Impact—Part 1: Ring Flutter and Ring Collapse and Their Effects on Gas Flow and Oil Transport," Proc. Inst. Mech. Eng., Part J, **216**(4), pp. 209–228.

[4] Tian, K.-T., 2002, "Dynamic Behaviours of Piston Rings and Their Practical Impact. Part 2: Oil Transport, Friction and Wear of Ring/Liner Interface and the Effects of Piston and Ring Dynamics," Proc. Inst. Mech. Eng., Part J, **216**(4), pp. 229–248.

[5] Baker, C. E., Theodossiades, S., Rahnejat, H., and Fitzsimons, B., 2012, "Influence of in-Plane Dynamics of Thin Compression Rings on Friction in Internal Combustion Engines," ASME J. Eng. Gas Turbines Power, **134**(9), p. 092801.

[6] Baker, C., Rahmani, R., Theodossiades, S., Rahnejat, H., and Fitzsimons, B., 2014, "On the Effect of Transient in-Plane Dynamics of the Compression Ring Upon Its Tribological Performance," ASME J. Eng. Gas Turbines Power, **137**(3), p. 032512.

[7] Baker, C., Theodossiades, S., Rahmani, R., Rahnejat, H., and Fitzsimons, B., 2017, "On the Transient Three-Dimensional Tribodynamics of Internal Combustion Engine Top Compression Ring," ASME J. Eng. Gas Turbines Power, **139**(6), p. 062801.

[8] Liu, Y., and Tian, T., 2017, "Development and Application of Ring-Pack Model Integrating Global and Local Processes—Part 1: Gas Pressure and Dynamic Behaviour of Piston Ring Pack," SAE Int. J. Engines, **10**(4), pp. 1927–1939.

[9] Liu, Y., Li, Y., and Tian, T., 2017, "Development and Application of Ring-Pack Model Integrating Global and Local Processes—Part 2: Ring-Liner Lubrication," SAE Int. J. Engines, **10**(4), pp. 1969–1983.

[10] Baker, C. E., Rahmani, R., Karagiannis, I., Theodossiades, S., Rahnejat, H., and Frendt, A., 2014, "Effect of Compression Ring Elastodynamics Behaviour Upon Blow by and Power Loss," SAE Paper No. 2014-01-1669.

[11] Bolander, N. W., Steenwyk, B. D., Sadeghi, F., and Gerber, G. R., 2005, "Lubrication Regime Transitions at the Piston Ring-Cylinder Liner Interface," Proc. Inst. Mech. Eng., Part J, **219**(1), pp. 19–31.

[12] Morris, N., Rahmani, R., Rahnejat, H., King, P. D., and Fitzsimons, B., 2013, "The Influence of Piston Ring Geometry and Topography on Friction," Proc. Inst. Mech. Eng., Part J., **227**(2), pp. 141–153.

[13] Ma, M. T., Sherrington, I., and Smith, E. H., 1997, "Analysis of Lubrication and Friction for a Complete Piston-Ring Pack With an Improved Oil Availability Model—Part 1: Circumferentially Uniform Film," Proc. Inst. Mech. Eng., Part J., **211**(1), pp. 1–15.

[14] Mishra, P. C., Balakrishnan, S., and Rahnejat, H., 2008, "Tribology of Compression Ring-to-Cylinder Contact at Reversal," Proc. Inst. Mech. Eng., Part J., **222**(7), pp. 815–826.

[15] Rahmani, R., Theodossiades, S., Rahnejat, H., and Fitzsimons, B., 2012, "Transient Elastohydrodynamic Lubrication of Rough New or Worn Piston Compression Ring Conjunction With an Out-of-Round Cylinder Bore," Proc. Inst. Mech. Eng., Part J., **226**(4), pp. 284–305.

[16] Akalin, O., and Newaz, G. M., 2001, "Piston Ring-Cylinder Bore Friction Modeling in Mixed Lubrication Regime—Part I: Analytical Results," ASME J. Tribol., **123**(1), pp. 211–218.

[17] Tian, T., Noordzij, L. B., Wong, V. W., and Heywood, J. B., 1998, "Modeling Piston-Ring Dynamics, Blowby, and Ring-Twist Effects," ASME J. Eng. Gas Turbines Power, **120**(4), pp. 843–854.

[18] Bewsher, S. R., Turnbull, R., Mohammadpour, M., Rahmani, R., Rahnejat, H., Offner, G., and Knaus, O., 2017, "Effect of Cylinder de-Activation on the Tribological Performance of Compression Ring Conjunction," Proc. Inst. Mech. Eng., Part J., **231**(8), pp. 997–1006.

[19] Baelden, C., and Tian, T., 2014, "A Dual Grid Curved Beam Finite Element Model of Piston Rings for Improved Contact Capabilities," SAE Int. J. Engines, **7**(1), pp. 156–171.

[20] Mishra, P. C., Rahnejat, H., and King, P. D., 2009, "Tribology of the Ring—Bore Conjunction Subject to a Mixed Regime of Lubrication," Proc. Inst. Mech. Eng., Part C, **223**(4), pp. 987–998.

[21] Furuhama, S., and Sasaki, S., 1983, "New Device for the Measurement of Piston Frictional Forces in Small Engines," SAE Paper No. 831284.

[22] Takiguchi, M., Sasaki, R., Takahashi, I., Ishibashi, F., Furuhama, S., Kai, R., and Sato, M., 2000, "Oil Film Thickness Measurement and Analysis of a Three Ring Pack in an Operating Diesel Engine," SAE Paper No. 2000-01-1787.

[23] Lamb, H., 1887, "On the Flexure and the Vibrations of a Curved Bar," Proc. London Math. Soc., **1**(1), pp. 365–377.

[24] Mayer, R., 1912, "Über Elastizität und Stabilität des geschlossenen und offenen Kreisbogens," Ph.D. thesis, BG Teubner, Berlin.

[25] Den Hartog, J. P., 1928, "The Lowest Natural Frequency of Circular Arcs," London, Edinburgh Dublin Philos. Mag. J. Sci., **5**(28), pp. 400–408.

[26] Brown, F. H., 1934, "Lateral Vibration of Ring-Shaped Frames," J. Franklin Inst., **218**(1), pp. 41–48.

[27] Love, A. E. H., 1944, *Treatise on Mathematical Theory of Elasticity*, Dover Publications, New York.

[28] Archer, R. R., 1960, "Small Vibrations of Thin Incomplete Circular Rings," Int. J. Mech. Sci., **1**(1), pp. 45–56.

[29] Volterra, E., and Morell, J. D., 1961, "Lowest Natural Frequency of Elastic Arc for Vibrations Outside the Plane of Initial Curvature," ASME J. Appl. Mech., **28**(4), pp. 624–627.

[30] Lang, T. E., 1962, "Vibration of Thin Circular Rings, Part 1," Jet Propulsion Laboratory, California Institute of Technology, Pasadena, CA, Report No. 32-261.

[31] Lang, T. E., 1963, "Vibration of Thin Circular Rings—Part II: Modal Functions and Eigenvalues of Constrained Semicircular Rings," Jet Propulsion Laboratory, California Institute of Technology, Pasadena, CA, Report No. JPL-TR-32-261.

[32] Ojalvo, I. U., 1962, "Coupled Twist-Bending Vibrations of Incomplete Elastic Rings," Int. J. Mech. Sci., **4**(1), pp. 53–72.

[33] Morley, L. S. D., 1958, "The Flexural Vibrations of a Cut Thin Ring," Q. J. Mech. Appl. Math., **11**(4), pp. 491–497.

[34] Rao, S. S., 1971, "Effects of Transverse Shear and Rotatory Inertia on the Coupled Twist-Bending Vibrations of Circular Rings," J. Sound Vib., **16**(4), pp. 551–566.

[35] Endo, M., 1972, "Flexural Vibrations of a Ring With Arbitrary Cross Section," Bull. JSME, **15**(82), pp. 446–454.

[36] Hawkings, D. L., 1977, "A Generalized Analysis of the Vibration of Circular Rings," J. Sound Vib., **54**(1), pp. 67–74.

[37] Yang, Y. B., and Kuo, S. R., 1987, "Effect of Curvature on Stability of Curved Beams," J. Struct. Eng., **113**(6), pp. 1185–1202.

[38] Dlugoš, J., and Novotný, P., 2014, "Computational Modelling of Piston Ring Dynamics in 3D," J. Middle Eur. Constr. Des. Cars, **12**(3), pp. 1–7.

[39] Bhimaraddi, A., 1988, "Generalized Analysis of Shear Deformable Rings and Curved Beams," Int. J. Solids Struct., **24**(4), pp. 363–373.

[40] Chidamparam, P., and Leissa, A. W., 1993, "Vibrations of Planar Curved Beams, Rings, and Arches," ASME Appl. Mech. Rev., **46**(9), pp. 467–483.

[41] Kang, K. J., Bert, C. W., and Striz, A. G., 1996, "Vibration and Buckling Analysis of Circular Arches Using DQM," Comput. Struct., **60**(1), pp. 49–57.

[42] Kijun, K., 2007, "Vibration Analysis of Thin-Walled Curved Beams Using DQM," J. Mech. Sci. Technol., **21**(8), pp. 1207–1217.

[43] Challamel, N., Casandjian, C., and Lerbet, J., 2009, "On the Occurrence of Flutter in the Lateral–Torsional Instabilities of Circular Arches Under Follower Loads," J. Sound Vib., **320**(3), pp. 617–631.

[44] Yang, F., Sedaghati, R., and Esmailzadeh, E., 2008, "Free in-Plane Vibration of General Curved Beams Using Finite Element Method," J. Sound Vib., **318**(4–5), pp. 850–867.

[45] Shahba, A., Attarnejad, R., Semnani, S. J., and Gheitanbaf, H. H., 2013, "New Shape Functions for Non-Uniform Curved Timoshenko Beams With Arbitrarily Varying Curvature Using Basic Displacement Functions," Meccanica, **48**(1), pp. 159–174.

[46] Luu, A.-T., Kim, N.-I., and Lee, J., 2015, "NURBS-Based Isogeometric Vibration Analysis of Generally Laminated Deep Curved Beams With Variable Curvature," Compos. Struct., **119**, pp. 150–165.

[47] Dowson, D., Ruddy, B. L., and Economou, P. N., 1983, "The Elastohydrodynamic Lubrication of Piston Rings," Proc. R. Soc. London, Ser. A, **386**(1791), pp. 409–430.

[48] Turnbull, R., Mohammadpour, M., Rahmani, R., Rahnejat, H., and Offner, G., 2017, "Coupled Elastodynamics of Piston Compression Ring Subject to Sweep Excitation," Proc. Inst. Mech. Eng., Part K, **231**(3), pp. 469–479.

[49] Rao, S. S., 2007, *Vibration of Continuous Systems*, Wiley, Hoboken, NJ.

[50] Rao, S. S., and Sundararajan, V., 1969, "In-Plane Flexural Vibrations of Circular Rings," ASME J. Appl. Mech., **36**(3), pp. 620–625.

[51] Bell, J. R., and Rothberg, S. J., 2000, "Rotational Vibration Measurements Using Laser Doppler Vibrometry: Comprehensive Theory and Practical Application," J. Sound Vib., **238**(4), pp. 673–690.